An unusual strolling motion of polar cap patches: an implication of the influence of tail reconnection on the nightside polar cap convection

K. Hosokawa[1,2], J. I. Moen[1], P. T. Jayachandran[3], K. Shiokawa[4], and Y. Otsuka[4]

[1] Dept. of Physics, Univ. of Oslo, Oslo, Norway
[2] Dept. of Comm. Eng. and Informatics, Univ. of Electro-Communications, Tokyo, Japan
[3] Dept. of Physics, Univ. of New Brunswick, Fredericton, Canada
[4] Solar-Terrestrial Environment Laboratory, Nagoya Univ., Nagoya, Aichi, Japan

Correspondence

Keisuke Hosokawa
Dept. of Comm. Eng. and Informatics
University of Electro-Communications,
Tokyo 182-8585, Japan

Tel: +81 424 43 5299
Fax: +81 424 43 5293

Email: hosokawa@ice.uec.ac.jp

For submission to *Journal of Geophysical Research*

Abstract. On January 12, 2005, a successive appearance of polar cap patches on the nightside was observed in the image captured by an all-sky imager (ASI) at Resolute Bay, Canada (74.73°N, 265.07°E). During the interval, the patches showed an unusual strolling motion in which their moving direction was very drastically changed twice (antisunward-dawnward-duskward). One may suspect that such changes in motion were caused by the reconfiguration of the polar cap convection due to a change in the IMF B_y. However, there were no remarkable variations in the sign of the IMF B_y in the solar wind data, which indicates that the unusual behavior of the patches was independent of the IMF-driven polar cap convection changes. Before the first change in the motion occurred, a transient bright aurora appeared in the equatorward part of the field-of-view in the dawn side. Immediately after the appearance of the transient auroral feature, the direction of the motion of the patches changed from anti-sunward to dawnward as if the patches were drawn into the aurora. After the disappearance of the aurora, the patches once almost stagnated but subsequently started to move duskward and anti-sunward. We interpret the bright auroral feature as a signature of the poleward boundary intensification (PBI), which is an ionospheric manifestation of an enhanced reconnection in the magnetotail. Accordingly, we speculate that an excited flow across the open-closed field line boundary redirected the anti-sunward polar cap convection towards the PBI and then allowed the patches to be drawn into the aurora near the polar cap boundary. This study indicates the importance of the tail reconnection as a driver of the nightside polar cap convection, resulting in the dynamical characteristics of polar cap patches; this relation may enable us to monitor the activity of the tail reconnection by using the motion of polar cap patches as an indicator.

1. Introduction

Polar cap patches, high-density plasma regions frequently appearing in the polar cap F region ionosphere, are believed to be generated in the vicinity of the dayside cusp inflow region when the interplanetary magnetic field (IMF) is directed predominantly southward [e.g., *Crowley*, 1996]. The horizontal extent of polar cap patches typically ranges from 100 km to 1000 km [*Coley and Heelis*, 1995], and the plasma density within each patch is often enhanced by a factor of 2–10 above that of the surrounding region [*Weber et al.,* 1984]. The dynamical properties of polar cap patches have been investigated by using an all-sky camera [*Weber et al.*, 1984], a coherent HF radar [*Milan et al.*, 2002], an incoherent scatter radar [*Pedersen et al.*, 2000], and an ionosonde [*MacDougall and Jayachandran*, 2007]. Numerous processes have been proposed to explain the generation of patches, such as the IMF-controlled reorientation of the cusp flow [*Milan et al.*, 2002], use of convection jets [*Rodger et al.*, 1994], in-situ plasma reduction under an intense electric field [*Valladares et al.*, 1994a], expansion of the polar cap convection pattern through pulsed reconnection [*Lockwood and Carlson*, 1992], and bursty plasma transport and patch cutting by FACs at subauroral latitudes [*Moen et al.*, 2006]. Most of the past studies suggested that once the patches are generated on the dayside, they survive for a long time and are transported anti-sunward over very long distances before they exit the polar cap into the nightside auroral zone.

As mentioned above, patches are believed to be transported over very long distances across the central polar cap before they convect into the nightside auroral zone. Thus, the motion of patches in the polar cap area follows the anti-sunward polar cap convection that is primarily dominated by upstream IMF conditions. *Hosokawa et al.* [2006, 2009b] demonstrated that changes in the speed and direction of the moving patches are in close correlation with the upstream IMF orientation. Specifically, the speed of patches is primarily controlled by the IMF B_z component and the direction of their drift velocities are well correlated with the IMF B_y component. However, some previous studies indicated that the motion of patches can also be influenced by nightside substorm activities. *Lorentzen et al.* [2004] first reported that the meridional drift speed of patches on the nightside was modulated by the auroral substorm phases. They presented a case in which the drift speed of the patches was high during the expansion and early recovery phase and gradually decreased in the late recovery phase. They interpreted this difference in terms of excitation of the convection near the nightside open-closed field line boundary. Later, *Wood et al.* [2009] showed that the separation of patches was also affected by the substorm activity. They suggested that the variation in the patch separations resulted from the expansion and contraction of the high-latitude plasma convection pattern on the nightside in response to the substorm activity.

In this paper, we report an event during which patches, detected by an all-sky airglow imager located in the northern part of Canada at Resolute Bay, showed an unusual strolling motion. Such an extraordinary behavior of polar cap patches has not been reported in previous studies. More interestingly, during the interval, an intense substorm occurred in the midnight sector. We discuss the cause of such an unusual motion of patches with regard to the reconfiguration of the background convection pattern associated with a change in the upstream IMF orientation and also with regard to the ongoing reconnection in the magnetotail. This paper is organized as follows. In section 2, we describe the dataset used in this study. Section 3 introduces the strolling motion of the polar cap patches detected using the all-sky imager. In section 4, we discuss the cause of such an unusual strolling motion. Section 5 provides a summary of this paper.

2. Instruments

The all-sky imager (ASI) used in this study has been in operation at Resolute Bay, Canada (74.73°N, 265.07°E; AACGM latitude 82.9°) since January 2005 [*Hosokawa et al.*, 2006] as a part of the Optical Mesosphere Thermosphere Imagers (OMTIs) system [*Shiokawa et al.*, 1999]. The ASI has numerous optical filters such as 557.7 nm, 630.0 nm, 777.4 nm, Na-line, and OH-band; this enables us to study various upper atmospheric phenomena occurring in the polar cap region, such as polar cap patches [*Hosokawa et al.*, 2006; 2009a; 2009b; 2010a; 2011b], tongue of ionization [*Hosokawa et al.*, 2009c; 2010b], polar cap aurora [*Koustov et al.*, 2008; *Jayachandran et al.*, 2009b; *Hosokawa et al.*, 2011a], and gravity waves at mesospheric heights [*Suzuki et al.*, 2009]. In this study, ASI images at a wavelength of 630.0 nm (OI6300, emission altitude ranges from 200 to 300 km), obtained every 2 min with an exposure time of 30 s, are employed for tracking the motion of polar cap patches.

In conjunction with the optical observations of patches, we investigate the background plasma drift obtained from digital ionosonde convection measurements using the Canadian Advanced Digital Ionosonde (CADI) at Resolute Bay [*MacDougall and Jayachandran*, 2001]. The CADI, presently operating as part of the Canadian High Arctic Ionospheric Network (CHAIN) [*Jayachandran et al.*, 2009a], is a modern digital ionosonde, capable of providing ionospheric drift measurements along with conventional ionograms. The CADI employs an antenna array consisting of four short dipoles arranged along the sides of a square 30 m on each side; one receiver is dedicated to each antenna. Fixed frequency Doppler samples with 64 data points are obtained at 30 s intervals. The convection velocity (speed and azimuth) is then determined by processing the fixed frequency Doppler samples obtained from the four antennae. For details of the convection measurement with CADI, refer to *Grant et al.* [1995].

3. Observations

The interval presented is a 2-h period from 0930 to 1130 UT on January 12, 2005, during which polar cap patches observed over Resolute Bay showed unusual strolling motion. Figure 1a shows an example of the 630.0 nm all-sky airglow image captured at 1010 UT. To indicate the slight enhancement in the airglow intensity caused by patches, the airglow distribution is shown as percentage deviation from a 1-h running average [*Hosokawa et al.*, 2010a]. At this time, four individual patches (A–D) can be identified within the field-of-view (FOV) of the ASI. Patch A, the most prominent of the four, was located near the zenith. The other three (B, C, and D) were observed at a lower elevation in the northwestern part of the FOV. As will be discussed in detail later in this section, these patches first appeared from the northern edge of the FOV, drifted westward along the horizon, and suddenly started moving southeastward along the dashed line in Figure 1a (SE–NW cross section). After they passed through the zenith, they completely reversed their moving direction and drifted northwestward.

In order to analyze the changes in the direction of the patches in greater detail, we plot the optical data as a keogram along the SE–NW cross section in Figure 1c. Patch A appeared at around 0930 UT in the northwestern edge of the FOV, stayed near the horizon for a while, and then started moving southeastward at around 0954 UT. The vertical dashed line indicates the time at which patch A arrived at the zenith of Resolute Bay, as shown in Figure 1a. At around 1024 UT, patch A almost stopped its southeastward motion and started moving northwestward. This reversal of patch motion is most clearly recognized in the keogram, where the trace of patch

A resembles the Roman letter "V." If we take a closer look at the keogram, however, there are indications of V-shaped traces for patches B, C, and D, suggesting that all the patches within the FOV reversed their moving direction at around 1024 UT. There exist several bright traces before 0950 UT and after 1045 UT near the zenith. These features are not associated with polar cap patches but correspond to polar cap arcs that are generally observed during the northward IMF intervals [*Valladares et al.*, 1994b; *Hosokawa et al.*, 2011a].

Figure 1b shows the same data as those displayed in Figure 1a. Here, however, the raw all-sky image has been converted into the altitude adjusted corrected geomagnetic (AACGM) coordinates [*Baker and Wing*, 1989] assuming an emission height of 250 km and then mapped into coordinates of magnetic local time (MLT) and magnetic latitude (MLAT). Magnetic midnight is at the bottom, and the dotted circle represents an MLAT of 80°. At this time, patch A was located in the middle of the FOV, above 80° MLAT at around 03 MLT. The SE–NW cross section shown in Figure 1a is superimposed as the dashed line, which is almost parallel to the dawn-dusk direction. Hence, the patches first appeared from the sunward part of the FOV, drifted anti-sunward along the edge of the FOV for a while, and eventually started drifting dawnward. After the reversal at 1024 UT, they drifted predominantly duskward. Since patches are generally known to drift in the anti-sunward direction along the streamline of the polar cap convection, the motion of the patches in the dusk-dawn direction during the present interval is extraordinary.

Figure 2 shows a sequence of the 630.0 nm all-sky airglow images obtained at 4 min intervals from 0940 UT to 1056 UT. At 0940 UT (image a), patch A appeared from the northern edge of the FOV and drifted westward almost along the horizon until 0952 UT (image d). At 0956 UT (image e), patch A turned around and started moving southeastward. This southeastward motion of patch A continued until it was completely reversed at 1024 UT (image l). Patches B, C, and D appeared slightly later from the northern edge of the FOV and moved along the direction of the zenith until the reversal. Immediately after the reversal at 1024 UT, the patches started moving northwestward and, eventually, almost moved out of the FOV by 1044 UT (image q). After the disappearance of the patches, polar cap arcs appeared from the south and filled the FOV until the end of this sequence. An animation showing the temporal evolution of the patches during a 3-h interval from 0900 UT to 1200 UT at a rate of one frame every 2 min accompanies the electronic version of this article (Animation 1). This animation sequence more clearly demonstrates the drastic changes in the moving direction of the patches.

The top panel of Figure 3 summarizes the trajectory of patch A from 0940 UT to 1050 UT within the all-sky FOV. To formulate this plot, we identified the center of patch A in the all-sky images every 2 min. As mentioned above, patch A appeared from the northern edge of the FOV and first drifted westward along the horizon. At 0954 UT, patch A changed its moving direction clockwise and moved southeastward until the reversal at 1024 UT. After the reversal, patch A drifted northwestward until it almost disappeared from the FOV at 1050 UT. The bottom panel of Figure 3 shows the same trajectory data as those displayed in the top panel. In the bottom panel, however, the trajectory is mapped into coordinates of MLT and MLAT. Magnetic midnight is at the bottom, and the dotted circle represents an MLAT of 80°. After patch A appeared it drifted anti-sunward until 0954 UT, which is an usual motion for patches in southward IMF conditions. After the first redirection of patch motion at 0954 UT, patch A drifted predominantly dawnward and, interestingly, moved somewhat sunward (i.e., backward). After the reversal at 1024 UT, patch A again started moving duskward toward the midnight.

To investigate the changes in patch motion in a more quantitative way, we estimate the velocity of the patches using a patch-tracking algorithm developed by *Hosokawa et al.* [2006]. This method is based on two-dimensional cross-correlation analysis of consecutive all-sky images. Using this algorithm, we can automatically derive the speed and direction of patches at 25 points near the zenith [*Hosokawa et al.*, 2009b]. In the right panel of Animation 1, the estimated velocity vectors are superimposed on the all-sky images as red arrows. The animation sequence clearly demonstrates that the estimated motion vectors accurately trace the actual motion of the patches. Figure 4b and c shows, respectively, the magnitude and azimuth of the estimated patch velocity. Note that the velocity azimuth is at an angle clockwise from the geographic pole; thus, the velocity azimuth of 90° corresponds to the motion toward the geographic east. For the sake of comparison, we again plot the keogram of the optical data along the SE–NW cross section in Figure 4a. It should be emphasized that the velocities before 1000 UT and after 1045 UT do not represent the motion of patches because they were located near the horizon far away from the points where the velocity was estimated.

The velocity magnitude varied from 200 to 500 m s^{-1} during the passage of the patches. At around 1010 UT, at which patch A was detected near the zenith, its speed was ≈450 m s^{-1}. Then, the speed of the patches once slowed down to ≈200 m s^{-1} around 10 min before the reversal and increased again immediately after the reversal. The azimuth ranged from 100° to 140° before the reversal (1000–1020 UT), which is consistent with the southeastward motion of the patches. About 4 min before the reversal, the velocity azimuth started rotating counter clockwise and then turned to negative when the reversal occurred. After the reversal, the azimuth was around 50°, which again is in good agreement with the northwestward motion of the patches. The grey points in Figure 4b and c represent the plasma drift obtained from the CADI at Resolute Bay. The data appear scattered especially after the reversal, which is probably because the CADI did not receive sufficient echoes from the patches after the reversal, owing to their diffuse spatial structure. Nevertheless, before the reversal, the azimuth values obtained from the CADI were in good agreement with those from the optics, suggesting that the motion of the patches corresponded to the background convection.

4. Discussion

In this section, we discuss the cause of the unusual strolling motion of the patches with regard to the change in the background convection pattern. It is well known that polar cap patches are observed mostly during southward IMF conditions [*Hosokawa et al.*, 2009b]. In such conditions, the anti-sunward convection is established in the polar cap due to an enhanced tailward transfer of newly-opened magnetic fluxes by the dayside magnetopause reconnection. However, the polar cap flow occasionally exhibits significant distortion toward dusk or dawn, even during southward IMF intervals, depending on the sign of the IMF B_y [e.g., *Cowley et al.*, 1991]. Hence, it is possible that the changes in patch motion were simply due to a reconfiguration of the polar cap convection pattern associated with the change in the IMF B_y. If there are large-scale variations in the sign of the IMF B_y, the balance between the two convection cells will change, and consequently, patches may be transported in a different direction.

Figure 5a–d shows, respectively, the solar wind velocity, proton density, IMF B_y, and IMF B_z during a 2-h period from 0900 UT to 1100 UT; these parameters were obtained from the ACE spacecraft located far upstream of the Earth ($X_{GSM} \approx 228$ R_E). A solar wind velocity of ≈590 km s^{-1} and a proton density of ≈12 cc^{-1} were measured during the strolling motion of the patches, implying a delay of 45 min between the spacecraft location and the dayside subsolar magnetopause [*Khan and Cowley*, 1999]. Additional time delay should be considered to account for the delay from the subsolar magnetopause to the nightside polar cap. *Bahcivan et al.* [2010] employed incoherent scatter radar data obtained at Resolute Bay to estimate the response of the polar cap flow to the southward turning of the IMF. They examined 10 events of clear southward turning of the IMF and derived an average response time of 13 min. Further evidence was recently provided by *Hosokawa et al.* [2011b], who reported a delay of around 15 min between the arrival of the IMF variation and its influence on the patch motion. Thus, in Figure 5a–d, the time-series have been shifted by 58 min (45 + 13 min).

IMF B_y in Figure 5c was negative almost throughout this interval. IMF B_z in Figure 5d changed its orientation more frequently, although it was predominantly negative during the interval of the strolling motion except for a brief positive excursion from 1012 UT to 1020 UT, which is a favorable condition for the generation of patches near the cusp and their subsequent delivery toward the nightside polar cap. In order to investigate the IMF variation during the strolling motion in greater detail, the IMF B_y and B_z obtained from ACE are again plotted for a 1-h interval from 0940 to 1040 UT; this plotting is shown in the lower two panels of Figure 5. During this 1-h period, we identified two drastic changes in the moving direction of the patches, at 0954 and 1024 UT. These timings are denoted by vertical dashed lines in Figure 5e and f. As mentioned above, one of the possible explanations for the changes in patch motion is the reconfiguration of the polar cap convection associated with a sudden polarity change of the IMF B_y. However, as seen in Figure 5e, IMF B_y was continuously negative and exhibited no large-scale change in its polarity at around both 0954 UT and 1024 UT. This implies that the strolling motion of the patches was independent of the IMF-driven polar cap convection changes. This suggests that a certain process, which is not associated with the dayside reconnection, probably modified the polar cap flow and caused the changes in the patch motion. Since the existence of such a process can probably be evidenced in the original all-sky images, we revisited the optical data; the details are discussed as follows.

Taking a closer look at the all-sky images (Figure 2), we found that a bright feature appeared near the southeastern edge of the FOV at 0952 UT (image d), which was just a few minutes before the first change of the patch moving direction at 0954 UT. This feature brightened in the subsequent three images (Figure 2e–g) and continued to be seen until 1012 UT (image i). At 1008 UT (image h), this bright optical feature could clearly be observed to be in the form of an auroral arc; thus, it was probably a signature of auroral intensification near the nightside polar cap boundary. Immediately after the appearance of the bright auroral feature, patch A changed its moving direction toward southeast. After that, patch A drifted southeastward as if it was drawn to the bright aurora occurring at the opposite side of the FOV. It may be difficult to see such an attractive force of the aurora on patch A in the snapshots in Figure 2. However, the animation attached to the electronic version more clearly demonstrates that patch A turned around immediately after the auroral intensification occurred and got pulled into the aurora. More interestingly, just after the disappearance of the aurora at around 1012 UT, the southeastward motion of patch A slowed down significantly (Figure 4b) and almost stagnated. This again indicates that the appearance of the aurora contributed to the motion of the patches. About 10 min after the disappearance of the bright auroral feature, the patches started moving again and drifted northwestward.

Now, we discuss the origin of the bright auroral feature that seemed to affect the motion of the patches in the polar cap area. One prospective reason for the origin of the bright auroral feature is a poleward boundary intensification (PBI) [*Lyons et al.*, 1999], which is known to be an intense, transient auroral disturbance that initiates at the nightside polar cap boundary [*Zesta et al.*, 2002]. PBIs have been related to enhanced flows that carry plasma across the nightside open-closed field line boundary [*de la Beaujardière et al.*, 1994] into the plasma sheet [*Lyons et al.*, 1999]. Specifically, PBIs are considered to be a signature of fast earthward flows in the magnetotail, referred to as bursty bulk flows (BBFs) [*Angelopoulos et al.*, 1992]. *Zesta et al.* [2002] reported a one-to-one correlation between PBIs and BBFs. More recently, *Nishimura et al.* [2010] demonstrated that longitudinally narrow flow bursts in the nightside polar cap can precede PBIs that are followed by equatorward moving north–south (N–S) arcs, including those leading to a substorm onset. They suggested that the high occurrence rate of PBIs and N–S arcs before the substorm onset suggests a preceding magnetic reconnection near the nightside open-closed field line boundary. *Lyons et al.* [2010] showed, by using the THEMIS observations, that such enhanced flows across the plasma sheet boundary layer are often seen a few minutes prior to onset.

Figure 6 shows a stack plot of the H-component ground magnetic field variation obtained from 8 stations of the Geophysical Institute Magnetometer Array (GIMA) magnetometer chain. These ground magnetometer stations were located at around 23 MLT during the strolling motion of the patches. The data show negative deflection starting at 1005 UT, indicating that a substorm occurred on the nightside. The onset of the substorm was about 10 min after the appearance of the bright auroral feature. This information supports the speculation that the bright auroral feature in the southeastern part of the FOV was a possible signature of PBI near the open-closed field line boundary. As reported by *Nishimura et al.* [2010] and *Lyons et al.* [2010], the bright auroral feature was probably accompanied by a burst of equatorward flow across the open-close field line boundary due to an enhanced localized reconnection in the magnetotail. Such an enhanced flow across the boundary could excite the flow even within the polar cap, as described by *Cowley and Lockwood* [1992] and *Grocott et al.* [2002]. As a result, the anti-sunward polar cap flow was redirected toward the region of the flow burst in the vicinity of the PBI, which allowed the patches to be drawn into the region of the bright aurora.

The possible signature of PBI disappeared at 1010 UT (Figure 2i), which indicates that the enhancement of tail reconnection ceased at the time. This suggests that the motion of the patches was not dominated by the tail reconnection any longer. In such a situation, the patches could drift along the streamline of the IMF-driven polar cap convection. In actual, however, the patches did not move in any specific direction for ≈10 min. This is probably because the IMF B_z was directed positive in this interval. Thus, neither dayside nor nightside reconnection could drive the convection in the polar cap, and then, the convection came to a halt during this stagnation of the patches. At 1020 UT, the IMF B_z became negative again. In addition, the IMF B_y started changing toward positive which could introduce a duskward component in the anti-sunward polar cap convection [e.g., *Hosokawa et al.*, 2006]. Hence, after 1024 UT, the patches again started moving duskward toward the normal exit of the twin-cell polar cap convection, which may extend for all MLT hours between 1830 and 0530 MLT but is mostly located around 23 MLT [*Moen et al.*, 2007]. That is, the drastic reversal of the patch moving direction at 1024 UT was caused by a convolution of the effects of the dayside and nightside reconnections on the polar cap convection. The other thing worth noting is that the timing of the reversal at 1024 UT was very close to the start of the substorm recovery phase (Figure 6). *Baumjohann et al.* [1999] demonstrated that the start of the recovery phase is caused by a stop of tail reconnection as the pileup of dipolarized magnetic field reaches near-earth reconnection site. This also suggests that the reversal of the patches was somehow related to the stop of tail reconnection. This interpretation is consistent with the report by *Lorentzen et al.* [2004] that polar cap patches were occasionally drawn into the auroral oval during episodes of tail reconnection. The current observations also suggest that the motion of patches can be altered by the ongoing tail reconnection activities, which may enable us to monitor the status of tail reconnection from the motion of polar cap patches.

In this paper, we suggest that the motion of polar cap patches on the nightside can be affected by the occurrence of bursty tail reconnection. We assume that tail reconnection can change the plasma convection even in the region of open field lines. In actual, recent observations demonstrated that enhancements of the flow are often seen near the nightside polar cap boundary a few minutes prior to onset [*Nishimura et al.*, 2010; *Lyons et al.*, 2010]. However, it is still unclear whether tail reconnection can change the polar cap flow in the region relatively distant from the open-closed field line boundary. In this sense, we have to remind ourselves that the current interpretation is nothing more than one of the possible scenarios. During the interval studied, however, the solar wind data indicate that the strolling motion of the patches cannot be explained by changes in the polar cap flow caused by the dayside process; thus, we have to understand this unusual motion somehow in terms of the nightside process. In order to evaluate the impact of tail reconnection on the polar cap flow, now we are statistically investigating the variation of the polar cap convection estimated from the ASI at Resolute Bay by using the method of *Hosokawa et al.* [2006] near substorm onsets.

5. Summary

We reported an occurrence of polar cap patches, detected by an all-sky airglow imager (ASI) located on the nightside, showing an unusual strolling motion in which the direction of their motion is drastically changed twice. The patches once changed their moving direction from anti-sunward to dawnward. About 30 min after the first change of the motion, the patches almost reversed their moving direction and again started the duskward and anti-sunward drift toward the midnight local time sector. One possible explanation for such changes in patch motion is a reconfiguration of the polar cap convection, especially a variation in the dawn-dusk component of the plasma flow, due to a change in the IMF B_y polarity. The solar wind data obtained from the ACE spacecraft, however, show that there were no remarkable changes in the sign of the IMF B_y. This suggests that the unusual strolling motion of the patches was independent of the IMF-driven polar cap convection changes on the dayside. 1–2 min before the first change of the patch motion, a very bright auroral feature was observed in the southeastern part of the field-of-view (FOV) of the ASI, which could be a signature of some auroral intensification near the open-closed field line boundary. Immediately after the appearance of the auroral feature, the patches clearly changed their moving direction from anti-sunward to dawnward as if they were drawn to the bright aurora occurring at the opposite side of the FOV. After the disappearance of the aurora, the dawnward motion of the patches slowed down and the patches eventually restarted drifting anti-sunward. Since a substorm occurred ≈10 min after the appearance of the bright auroral feature, we interpret it as a signature of a poleward boundary intensification (PBI), which is an ionospheric manifestation of an enhanced reconnection in the magnetotail.

Then, we suggest that an enhanced flow across the open-close field line boundary excited the flow even within the polar cap and that the anti-sunward polar cap flow was redirected toward the region of the PBI. Consequently, the patches were drawn into the region of enhanced flow in the vicinity of the PBI. This interpretation indicates the importance of the nightside reconnection as a driver of the polar cap convection, resulting in the dynamical characteristics of the polar cap patches. This relation also suggests that we may be able to monitor the activity of tail reconnection using the motion of polar cap patches as a tracer.

Acknowledgments. This work was supported by Grants-in-Aid for Scientific Research (16403007, 19403010, 20244080 and 20740282) from the Japan Society for the Promotion of Science (JSPS). This work was carried out by the joint research program of the Solar-Terrestrial Environment Laboratory (STEL), Nagoya University. The authors thank M. Satoh, Y. Katoh, H. Hamaguchi, and Y. Yamamoto of STEL, Nagoya University, for their helpful support in airglow imaging observations. Special thanks are extended to staff of the Narwhal Arctic Service at Resolute Bay for kind and helpful support in operating the optical instrument. The optical observation at Resolute Bay was also supported by the NSF cooperative agreement ATM-0608577. Infrastructure funding for CHAIN was provided by the Canada Foundation for Innovation and the New Brunswick Innovation Foundation. CHAIN operation is conducted in collaboration with the Canadian Space Agency. The authors wish to thank N. Ness at the Bartol Research Institute for access to data from MFI and SWE instruments onboard the ACE spacecraft. GIMA data is provided by the Geophysical Institute of the University of Alaska Fairbanks. This work was done while K.H. was staying at Department of Physics, University of Oslo as a guest researcher. His research at University of Oslo was supported by a grant of "Excellent Young Researcher Overseas Visit Program" from JSPS. JM has been received support from the Norwegian Research Council, the AirForce Office of Scientific Research, Air Force Material Command, USAF, under grant number FA8655-10-1-3003, and COST action ES0803.

References

Angelopoulos, V., et al. (1992), Bursty bulk flows in the central plasma sheet, *J. Geophys. Res., 97*, 4027.

Bahcivan, H., R. Tsunoda, M. Nicolls, and C. Heinselman (2010), Initial ionospheric observations made by the new Resolute incoherent scatter radar and comparison to solar wind IMF, *Geophys. Res. Lett., 37*, doi:10.1029/2010GL043632.

Baker, K. B., and S. Wing (1989), A new magnetic coordinate system for conjugate studies of high latitudes, *J. Geophys. Res., 94*, 9139.

Baumjohann, W., M. Hesse, S. Kokubun, T. Mukai, T. Nagai, and A. Petrukovich (1999), Substorm dipolarization and recovery, *J. Geophys. Res., 104*, 24,995-25,000.

Coley, W. R., and R. A. Heelis (1995), Adaptive identification and characterization of polar ionization patches, *J. Geophys. Res., 100*, 23,819.

Cowley, S. W. H., J. Morelli, and M. Lockwood (1991), Dependence of Convective Flows and Particle Precipitation in the High - Latitude Dayside Ionosphere on the X and Y Components of the Interplanetary Magnetic Field, *J. Geophys. Res., 96*, 5557.

Cowley, S. W. H. and M. Lockwood (1992), Excitation and decay of solar-wind driven flows in the magnetosphere-ionosphere system *Ann. Geophys., 10*, 103.

Crowley, G. (1996), Critical review of ionospheric patches and blobs, in *Review of Radio Science 1993-1996*, edited by W. R. Stone, Oxford University Press, New York, 619.

de la Beaujardière, O., et al. (1994), Quiet-time intensifications along the poleward auroral boundary near midnight, *J. Geophys. Res., 99*, 287.

Grant, I., J. MacDougall, J. Ruohoniemi, W. Bristow, G. Sofko, J. Koehler, D. Danskin, and D. Andre (1995), Comparison of plasma flow velocities determined by the ionosonde Doppler drift technique, SuperDARN radars, and patch motion, *Radio Sci., 30*, 1537.

Grocott, A., S. W. H. Cowley, J. B. Sigwarth, J. F. Watermann, and T. K. Yeoman (2002), Excitation of twin-vortex flow in the nightside high-latitude ionosphere during an isolated substorm, *Ann. Geophys., 20*, 1577.

Hosokawa, K., K. Shiokawa, Y. Otsuka, A. Nakajima, T. Ogawa, and J. D. Kelly (2006), Estimating drift velocity of polar cap patches with all-sky airglow imager at Resolute Bay, Canada, *Geophys. Res. Lett., 33*, 10.1029/2006GL026916.

Hosokawa, K., K. Shiokawa, Y. Otsuka, T. Ogawa, J.-P. St-Maurice, G. J. Sofko, D. A. Andre (2009a), The relationship between polar cap patches and field-aligned irregularities as observed with an all-sky airglow imager at Resolute Bay and the PolarDARN radar at Rankin Inlet, *J. Geophys. Res., 114*, 10.1029/2008JA013707.

Hosokawa, K., T. Kashimoto, S. Suzuki, K. Shiokawa, Y. Otsuka and T. Ogawa (2009b), Motion of polar cap patches: A statistical study with all-sky airglow imager at Resolute Bay, Canada, *J. Geophys. Res., 114*, 10.1029/2008JA014020.

Hosokawa, K., T. Tsugawa, K. Shiokawa, T. Otsuka, T. Ogawa and M. Hairston (2009c), Unusually elongated bright optical plume in the polar cap F region: is it a tongue of ionization?, *Geophys. Res. Lett., 36*, 10.1029/2009GL037512.

Hosokawa, K., J.-P. St.-Maurice, G. J. Sofko, K. Shiokawa, Y. Otsuka, and T. Ogawa (2010a), Reorganization of polar cap patches through shears in the background plasma convection, *J. Geophys. Res., 115*, doi:10.1029/2009JA014599.

Hosokawa, K., T. Tsugawa, K. Shiokawa, Y. Otsuka, N. Nishitani, T. Ogawa and M. Hairston (2010b), Dynamic temporal evolution of polar cap tongue of ionization, *J. Geophys. Res., in press.*

Hosokawa, K., J. I. Moen, K. Shiokawa, and Y. Otsuka (2010c), Motion of polar cap arcs, *J. Geophys. Res., in press.*

Hosokawa, K., J. I. Moen, K. Shiokawa, and Y. Otsuka (2010d), Decay of polar cap patch, *J. Geophys. Res., submitted.*

Jayachandran, P. T., et al. (2009a), Canadian High Arctic Ionospheric Network (CHAIN), *Radio Sci., 44*, doi:10.1029/2008RS004046.

Jayachandran P. T., K. Hosokawa, J. W. MacDougall, S. Mushini, R. B. Langley, and K. Shiokawa (2009b), GPS Total Electron Content Variations Associated with a Polar Cap Arc, *J. Geophys. Res., 114*, doi:10.1029/2009JA014916.

Khan, H., S. W. H. Cowley (1999), Observations of the response time of high-latitude ionospheric convection to variations in the interplanetary magnetic field using EISCAT and IMP-8 data, *Ann. Geophys., 17*, 1306.

Koustov, S. A., K. Hosokawa, N. Nishitani, T. Ogawa, and K. Shiokawa (2008), Rankin Inlet PolarDARN radar observations of duskward moving Sun-aligned optical forms, *Ann. Geophys., 26, 2711.*

Lockwood, M., and H. C. Carlson Jr. (1992), Production of polar cap electron density patches by transient magnetopause reconnection, *Geophys. Res. Lett., 19*, 1731.

Lorentzen, D.A., N. Shumilov and J. Moen (2004), Drifting airglow patches in relation to tail reconnection, *Geophys, Res. Lett., 31*, doi:10.1029/2003GL017785.

Lyons, L., T. Nagai, G. Blanchard, J. Samson, T. Yamamoto, T. Mukai, A. Nishida, and S.

Kokubun (1999), Association between Geotail plasma flows and auroral poleward boundary intensifications observed by CANOPUS photometers, *J. Geophys. Res., 104*, 4485.

Lyons, L. R., Y. Nishimura, X. Xing, V. Angelopoulos, S. Zou, D. Larson, J. McFadden, A. Runov, S. Mende, and K.-H. Fornacon (2010), Enhanced transport across entire length of plasma sheet boundary field lines leading to substorm onset, *J. Geophys. Res., 115*, doi:10.1029/2010JA015831.

MacDougall, J., and P. Jayachandran (2001), Polar cap convection relationships with solar wind, *Radio Sci., 36*, 1869.

MacDougall, J. W., and P. T. Jayachandran (2007), Polar patches: Auroral zone precipitation effects, *J. Geophys. Res., 112*, doi:10.1029/2006JA011930.

Milan, S. E., M. Lester, and T. K. Yeoman (2002), HF radar polar patch formation revisited: summer and winter variations in dayside plasma structuring, *Ann. Geophys., 20*, 487.

Moen, J., Carlson, H. C. Carlson, K. Oksavik, C. P. Nielsen, S. E. Pryse, H. R. Middleton, I. W. McCrea, and P. Gallop (2006), EISCAT observations of plasma patches at sub-auroral cusp latitudes, *Ann. Geophys., 24*, 2363-2374.

Moen, J., N. Gulbrandsen, D. A. Lorentzen, and H. C. Carlson (2007), On the MLT distribution of F-region polar cap patches at night, *Geophys. Res. Lett., 34*, doi:10.1029/2007/GL029632.

Nishimura, Y., et al. (2010), Preonset time sequence of auroral substorms: Coordinated observations by all-sky imagers, satellites, and radars, *J. Geophys. Res., 115*, doi:10.1029/2010JA015832.

Pedersen, T., B. Fejer, R. Doe, and E. Weber (2000), An incoherent scatter radar technique for determining two-dimensional horizontal ionization structure in polar cap F region patches, *J. Geophys. Res., 105*, 10,637.

Rodger, A. S., M. Pinnock, J. R. Dudeney, K. B. Baker, and R. A. Greenwald (1994), A new mechanism for polar patch formation *J. Geophys. Res., 99*, 6425.

Shiokawa, K., Y. Katoh, M. Satoh, M. K. Ejiri, T. Ogawa, T. Nakamura, T. Tsuda, and R. H. Wiens (1999), Development of optical mesosphere thermosphere imagers (OMTI), *Earth Planets Space, 51*, 887.

Shiokawa, K., Y. Katoh, M. Satoh, M. K. Ejiri, and T. Ogawa, (2000), Integrating-sphere calibration of all-sky cameras for nightglow measurements, *Adv. Space Res., 26*, 1025.

Shiokawa, K., Y. Otsuka, and T. Ogawa (2009), Propagation characteristics of nighttime mesospheric and thermospheric waves observed by optical mesosphere thermosphere imagers at middle and low latitudes, *Earth Planets Space, 61*, 479.

Suzuki, S., K. Shiokawa, K. Hosokawa, K. Nakamura, and W. K. Hocking (2009), Statistical characteristics of polar cap mesospheric gravity waves observed by an all-sky airglow imager at Resolute Bay, Canada, *J. Geophys. Res., 114*, doi:10.1029/2008JA013652.

Valladares, C., S. Basu, J. Buchau, and E. Friis-Christensen (1994a), Experimental evidence for the formation and entry of patches into the polar cap, *Radio Sci., 29*, 167.

Valladares, C., H. Carlson Jr., and K. Fukui (1994b), Interplanetary Magnetic Field Dependency of Stable Sun-Aligned Polar Cap Arcs, *J. Geophys. Res., 99*, 6247.

Weber, E. J., J. Buchau, J. G. Moore, J. R. Sharber, R. C. Livingston, J. D. Winningham, and B. W. Reinisch (1984), F layer ionization patches in the polar caps, *J. Geophys. Res., 89*, 1683.

Wood, A. G., S. E. Pryse, and J. I. Moen (2009), Modulation of nightside polar patches by substorm activity, *Ann. Geophys., 27*, 3923.

Zesta, E., E. Donovan, L. Lyons, G. Enno, J. S. Murphree, and L. Cogger (2002), Two-dimensional structure of auroral poleward boundary intensifications, *J. Geophys. Res., 107*, doi:10.1029/2001JA000260.

Figure Captions

Figure 1 (a) 630.0 nm all-sky image at 1010 UT on January 12, 2005. To indicate the slight enhancement in the airglow intensity caused by patches, the airglow distribution is shown as a percentage deviation from a 1-h running average. (b) Same data as those of Figure 1a, but the raw all-sky image is converted into AACGM coordinates [*Baker and Wing*, 1989] assuming an emission height of 250 km and mapped into coordinates of MLT and MLAT. Magnetic midnight is at the bottom, and the dotted circle represents an MLAT of 80°. (c) Keogram reproduced from 630.0 nm all-sky images along the SE–NW cross section shown in Figure 1a.

Figure 2 Sequence of 630.0 nm airglow images obtained at 4 min intervals from 0940 to 1056 UT. To indicate the slight enhancement in the airglow intensity caused by patches, the airglow distribution is shown as a percentage deviation from a 1-h running average.

Figure 3 (Top) Trajectory of the center of patch A in the all-sky FOV of the ASI. (Bottom) Same data as those of the top panel, but the trajectory of patch A is converted into AACGM coordinates [*Baker and Wing*, 1989] and then mapped into coordinates of MLT and MLAT. Magnetic midnight is at the bottom, and the dotted circle represents an MLAT of 80°.

Figure 4 (a) Keogram reproduced from 630.0 nm all-sky images along the SE–NW cross section shown in Figure 1a. (b, c) Magnitude and azimuth of the patch velocity, estimated using a patch-tracking algorithm developed by *Hosokawa et al.* [2006] (black line). The grey dots represent the magnitude and azimuth of the convection obtained from the CADI at Resolute Bay. The velocity azimuth is at an angle clockwise from the geographic pole; thus, velocity azimuth of 90° corresponds to the motion toward the geographic east.

Figure 5 (a–d) Solar wind speed, proton density, IMF B_y, and IMF B_z, obtained from the ACE spacecraft during a 2-h interval from 0900 to 1100 UT. The time-series is shifted by 58 min to account for the solar wind propagation delay from the spacecraft to the nightside polar cap (refer to text for details). (e–f) IMF B_y and IMF B_z, obtained from the ACE spacecraft during a 1-h interval from 0940 to 1040 UT. The two timings in which the patches change their moving direction are indicated by the dashed vertical line.

Figure 6 Stack plot of the H-component ground magnetic field variation obtained from 8 stations of the GIMA magnetometer chain. These ground magnetometer stations were located at around 23 MLT during the strolling motion of the patches.

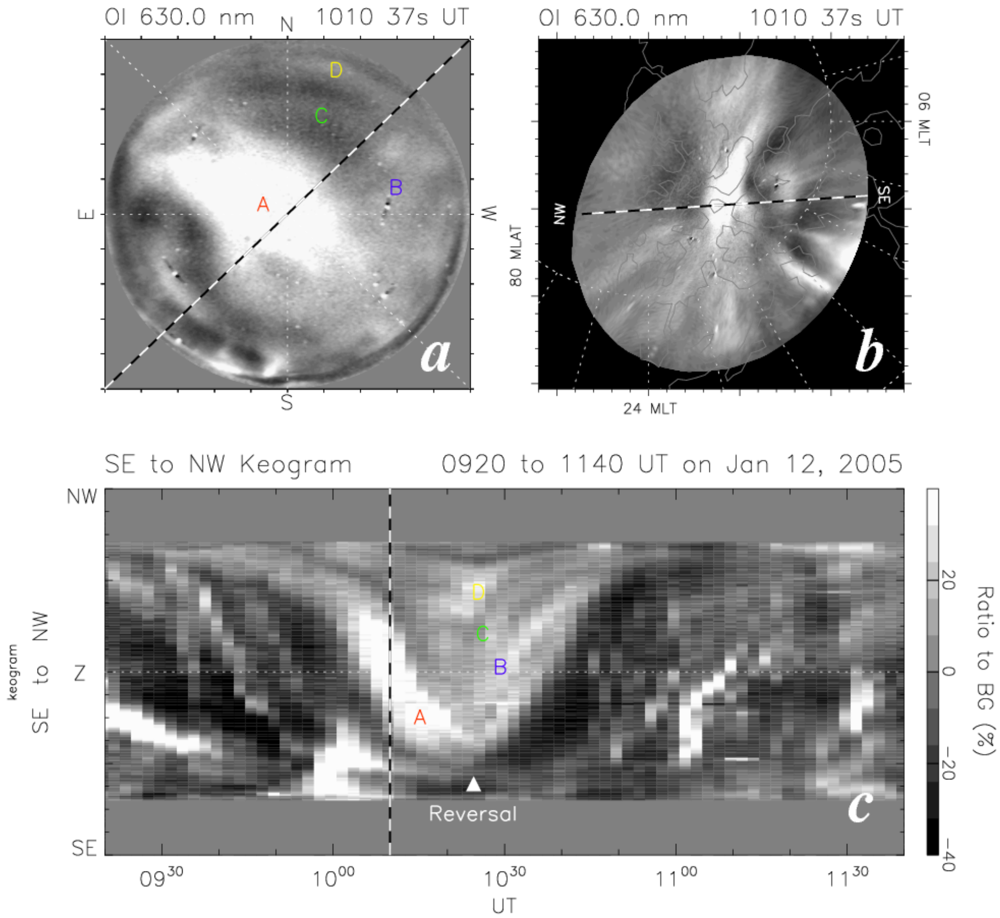
OI 630.0 nm
N
1010 37s UT
D
C
B
A
E
W
S
a
OI 630.0 nm
1010 37s UT
06 MLT
NW
SE
80 MLAT
24 MLT
b
SE to NW Keogram
0920 to 1140 UT on Jan 12, 2005
NW
Z
SE
keogram
SE to NW
D
C
B
A
Reversal
c
09^{30}
10^{00}
10^{30}
11^{00}
11^{30}
UT
20
0
−20
−40
Ratio to BG (%)

Figure 1

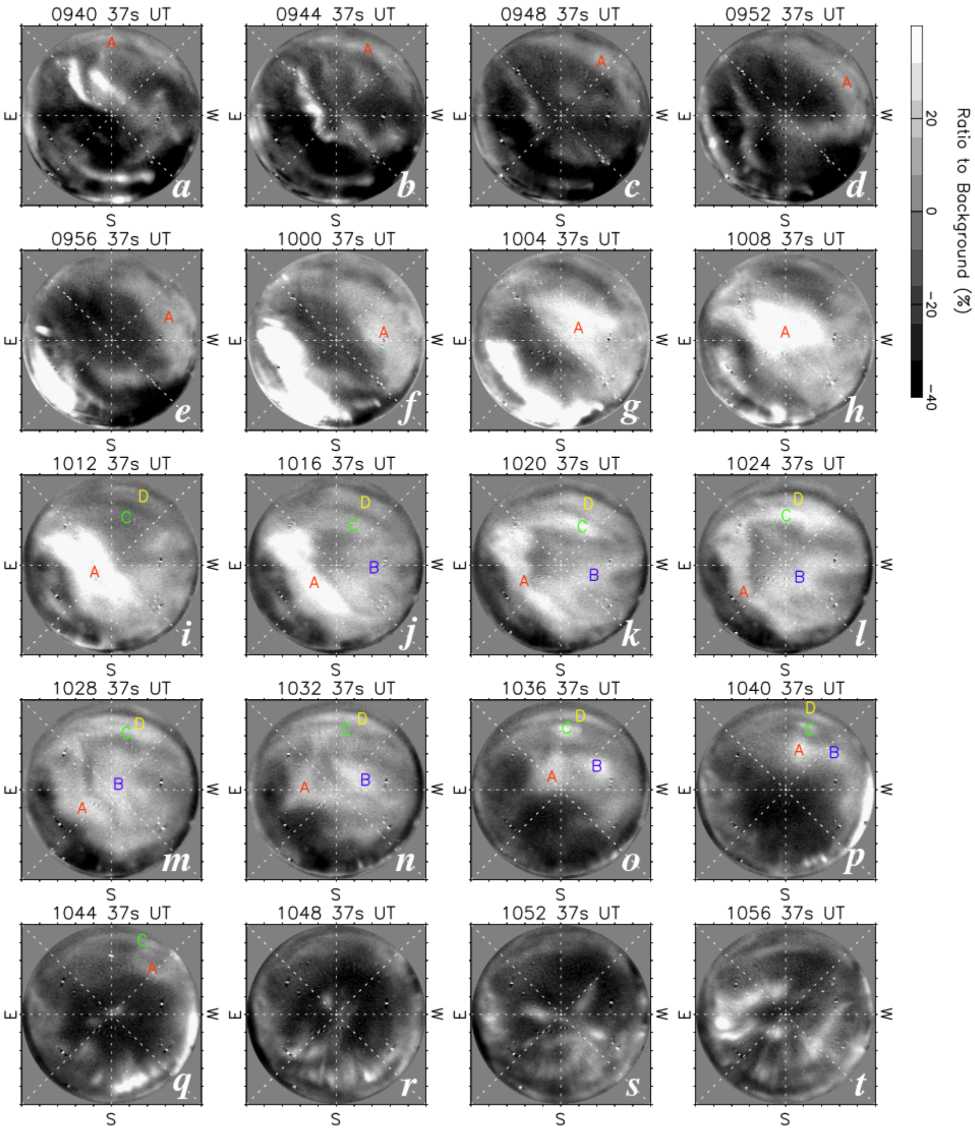
0940 37s UT
0944 37s UT
0948 37s UT
0952 37s UT
0956 37s UT
1000 37s UT
1004 37s UT
1008 37s UT
1012 37s UT
1016 37s UT
1020 37s UT
1024 37s UT
1028 37s UT
1032 37s UT
1036 37s UT
1040 37s UT
1044 37s UT
1048 37s UT
1052 37s UT
1056 37s UT
E
W
S
A
B
C
D
a
b
c
d
e
f
g
h
i
j
k
l
m
n
o
p
q
r
s
t
Ratio to Background (%)
20
0
−20
−40

Figure 2

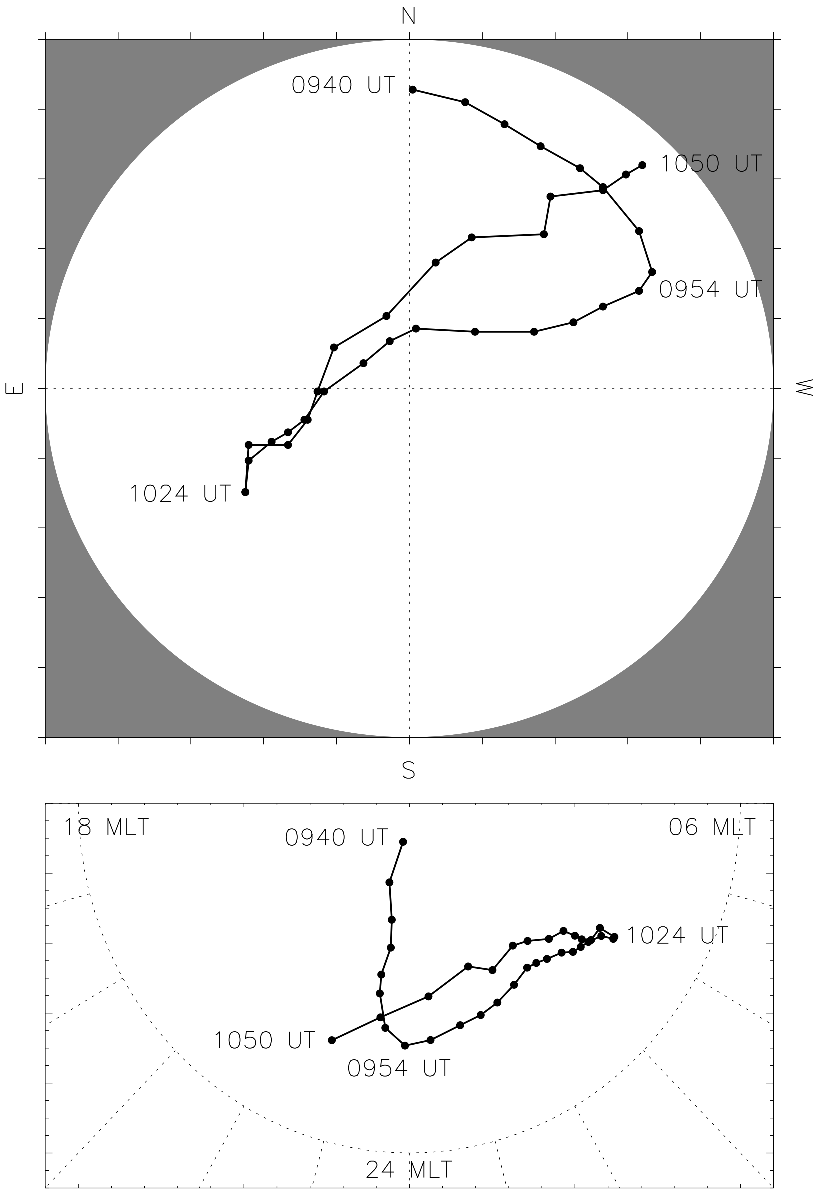
N
0940 UT
1050 UT
0954 UT
E
W
1024 UT
S
18 MLT
0940 UT
06 MLT
1024 UT
1050 UT
0954 UT
24 MLT

Figure 3

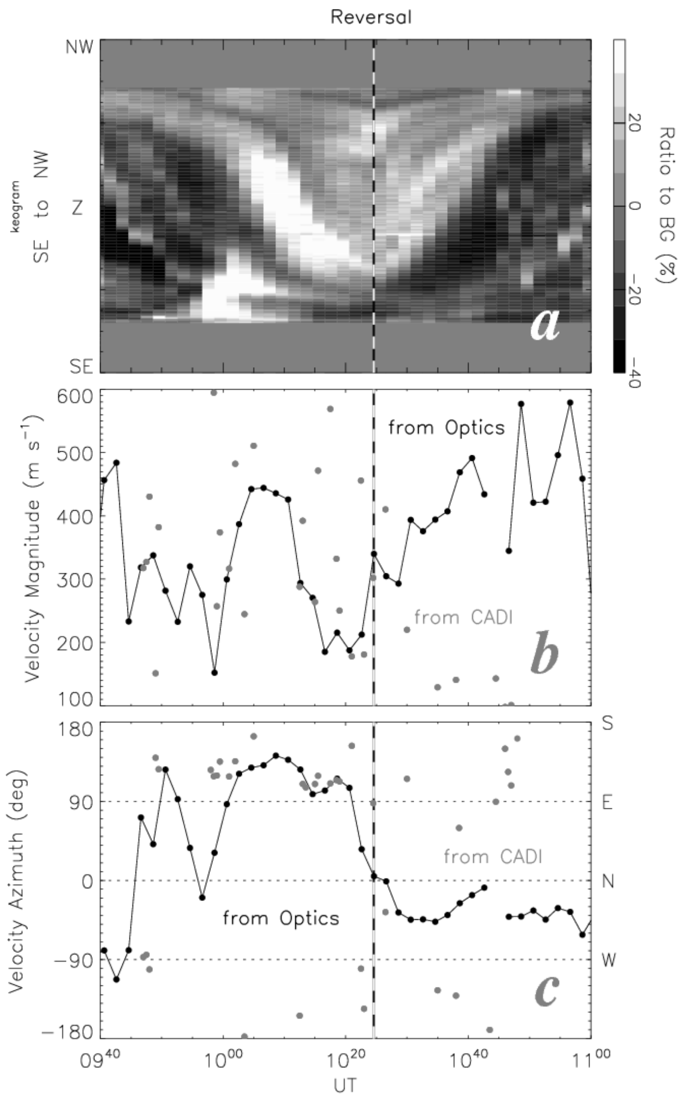

Reversal
NW
keogram SE to NW
Z
SE
Ratio to BG (%)
20
0
−20
−40
a
Velocity Magnitude (m s⁻¹)
from Optics
from CADI
b
Velocity Azimuth (deg)
S
E
N
W
from CADI
from Optics
c
UT

Figure 4

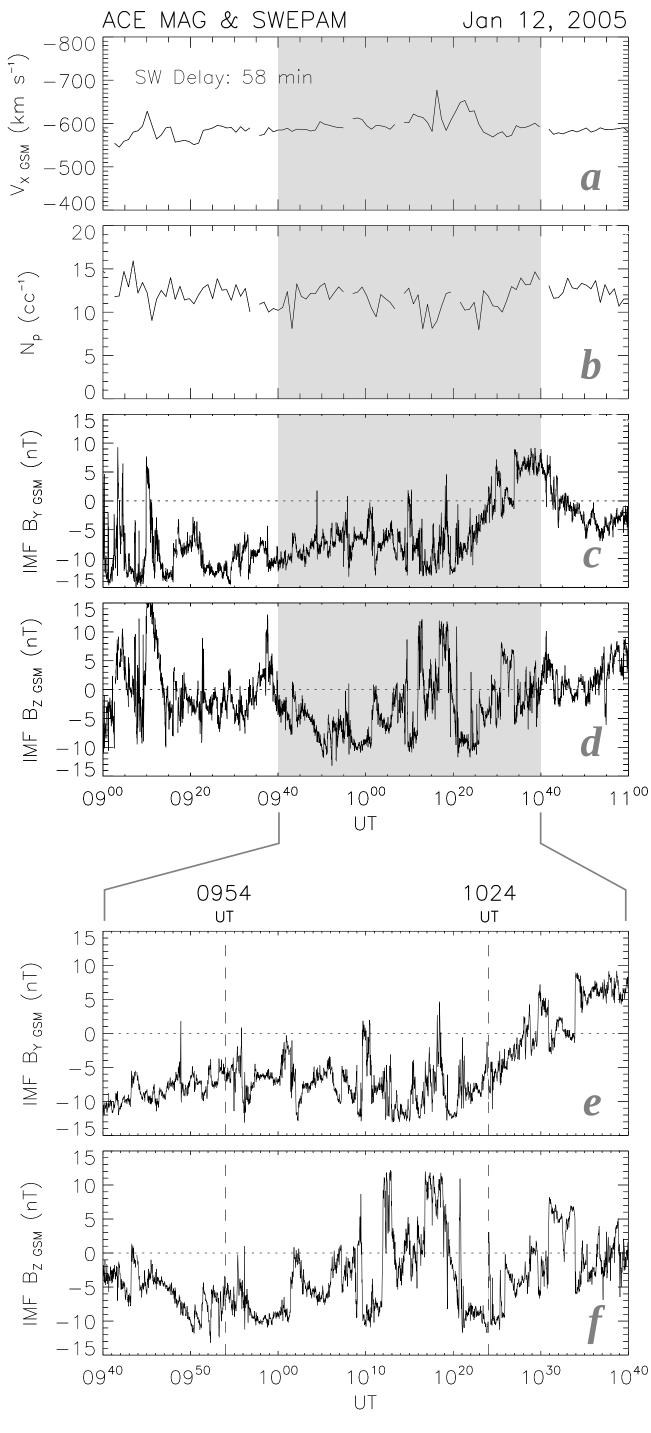
ACE MAG & SWEPAM
Jan 12, 2005
SW Delay: 58 min
V_X GSM (km s⁻¹)
N_p (cc⁻¹)
IMF B_Y GSM (nT)
IMF B_Z GSM (nT)
a
b
c
d
e
f
UT
0954 UT
1024 UT

Figure 5

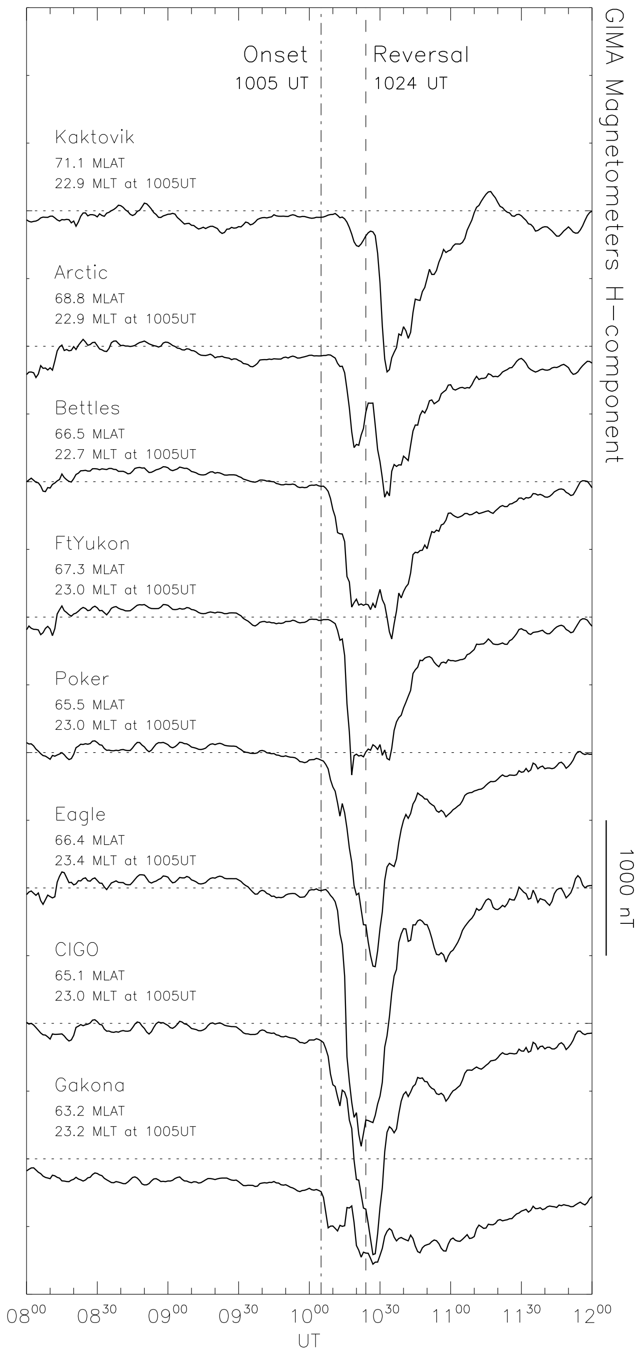
Onset
1005 UT
Reversal
1024 UT
GIMA Magnetometers H–component
Kaktovik
71.1 MLAT
22.9 MLT at 1005UT
Arctic
68.8 MLAT
22.9 MLT at 1005UT
Bettles
66.5 MLAT
22.7 MLT at 1005UT
FtYukon
67.3 MLAT
23.0 MLT at 1005UT
Poker
65.5 MLAT
23.0 MLT at 1005UT
Eagle
66.4 MLAT
23.4 MLT at 1005UT
CIGO
65.1 MLAT
23.0 MLT at 1005UT
Gakona
63.2 MLAT
23.2 MLT at 1005UT
1000 nT
08 00
08 30
09 00
09 30
10 00
10 30
11 00
11 30
12 00
UT

Figure 6